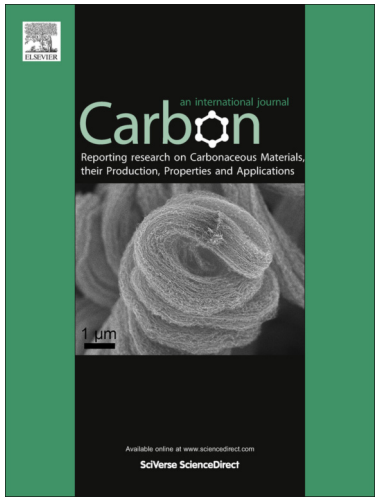

Morphology Engineering of Hollow Carbon Nanotube Pillars by Oxygen Plasma Treatment

Adrianus I. Aria, Bradley J. Lyon, Morteza Gharib

PII: S0008-6223(14)00922-1
DOI: http://dx.doi.org/10.1016/j.carbon.2014.09.070
Reference: CARBON 9367

To appear in: *Carbon*

Received Date: 6 August 2014
Accepted Date: 22 September 2014

Please cite this article as: Aria, A.I., Lyon, B.J., Gharib, M., Morphology Engineering of Hollow Carbon Nanotube Pillars by Oxygen Plasma Treatment, *Carbon* (2014), doi: http://dx.doi.org/10.1016/j.carbon.2014.09.070

Morphology Engineering of Hollow Carbon Nanotube Pillars by Oxygen Plasma Treatment

Adrianus I. Aria[1‡], Bradley J. Lyon[1‡], and Morteza Gharib[1*]

[1] Graduate Aerospace Laboratories, California Institute of Technology, Pasadena, CA 91125, USA

[‡] These authors contributed equally to this work

Abstract

Oxygen plasma treatment is introduced herein as a novel post-growth fabrication technique to engineer the macroscopic morphology of hollow carbon nanotube (CNT) pillars. Current fabrication techniques for patterned vertically-aligned CNTs only allow for the production of extruded structures with constant cross-sectional area. Oxygen plasma treatment is utilized to rectify this limitation by introducing variation to the cross-sectional area. The results presented herein demonstrate that a conical geometry can be successfully introduced by oxygen plasma treatment to a hollow cylindrical CNT pillars. Using oxygen plasma treatment, the blunt tip of a cylindrical CNT pillar can be controllably sharpened until it reaches a size reduction of more than 93%. A geometric model is presented herein to predict the morphology transformation of a hollow cylindrical CNT pillars during the oxygen plasma treatment. Three distinct phases of CNT structural and morphological evolution induced by oxygen plasma treatment are also identified. A mild CNT functionalization by oxygen adsorbates occurs in the first phase. The

[*] Corresponding author: Morteza Gharib. Tel: (626) 395-4450 email: mgharib@caltech.edu

second phase is indicated by drastic changes in the macroscopic morphology of CNT pillars. Structural amorphization and collapse of the base of the CNT pillars take place in the final phase.

1. Introduction

Carbon nanotubes (CNTs) represent a multi-functional material with a unique set of structural, electrical, thermal, and fluidic properties that make them attractive for use in numerous applications. However, their widespread use to date has been restricted by a lack of methodology to shape and transport CNTs after their fabrication [1]. Patterned vertically-aligned CNTs, produced by standard nanofabrication techniques of catalyst deposition and chemical vapor deposition, can allow for CNTs to be used in a wide range of applications including stamps for nanoimprint lithography [2], microneedles for transdermal drug delivery [3, 4], superhydrophobic surfaces [5, 6], electrical and thermal interconnects for microelectronics [1, 7, 8], field emission sources [9, 10], and electrodes for energy storage [11, 12]. Nevertheless, current nanofabrication methodology for vertically-aligned CNTs is restricted to extruded geometries with constant cross-sectional area since the pattern of the CNTs is controlled by catalyst patterning on a planar substrate.

In this study, oxygen plasma treatment is introduced as a simple technique to increase the utility of vertically-aligned CNT pillars by enabling true three-dimensional morphology. Specifically, we demonstrate the use of oxygen plasma treatment to engineer the macroscopic morphology of CNT structures by introducing a tapered geometry to hollow cylindrical CNT pillars. The ability to introduce a tapered geometry is deemed critical to improve the performance and mechanical stability of CNT pillars in numerous applications, including microneedles, multi-length scale electrical and thermal interconnects, and nanoimprint

lithography. Control of the plasma dosage allows oxygen plasma treatments to be used effectively to induce macroscopic shape changes of the CNT pillar in a relatively non-destructive manner. The results presented herein elucidate the effect of oxygen plasma on the evolution of both the macroscopic morphology and the microscopic structure of CNT pillars. Together, the results demonstrate the cascading effect of oxygen plasma treatments from individual nanotubes to large-scale morphology transformations of the CNT pillar.

Oxygen plasma treatments are commonly used as an etching process for cleaning wafers from organic contaminants in top-down fabrication methods. Oxygen plasma treatments are also known as one of the most useful means to introduce oxygen functionalization on graphitic structures, including CNTs and graphene. Numerous previous studies have shown that oxygen plasma produces a large amount of oxygen containing radicals that are readily adsorbed by these materials [13-19]. The adsorption of oxygen alters the highly periodic π-bond networks of graphitic structures, which results in changes in their electrical, mechanical, chemical, and wetting properties. It has also been known that excessive exposure to oxygen plasma treatment often results in irreversible damage to the CNT structure. While oxygen plasma treatment has been used for years to modify the morphology of non-patterned vertically-aligned CNTs [11, 18, 20], its use to modify the morphology of patterned vertically-aligned CNTs, in particular hollow CNT pillars, is yet to be explored. Because of the relevance of patterned vertically-aligned CNTs, in particular hollow CNT pillars, to numerous applications, as mentioned earlier, it is imperative to elucidate the underlying mechanism governing such modification.

Three distinct phases of CNT structural and morphological evolution induced by oxygen plasma treatment are identified in this study. A mild CNT functionalization by oxygen adsorbates occurs in the first phase. The second phase is indicated by drastic changes in the

macroscopic morphology of CNT pillars. Structural amorphization and collapse of the base of CNT pillars take place in the final phase. The morphology evolution of the CNT pillar is approximated by a geometric model that can be used to effectively predict the shape of tapered pillars after oxygen plasma treatment. Altogether, the results presented herein demonstrate the potential of oxygen plasma treatment as a post-growth fabrication technique to engineer the macroscopic morphology of aligned CNT structures.

2. Materials and Methods

Pillars of vertically aligned multi-wall carbon nanotubes (CNT) are fabricated by thermal chemical vapor deposition (CVD) method. Aluminum oxide buffer (Kurt J. Lesker, 99.99% purity) and iron catalyst (Kurt J. Lesker, 99.95% purity) layers are patterned on silicon wafers (El-Cat Inc., polished 300nm thermal oxide) prior to the CNT growth using standard photolithography and e-beam evaporation (CHA Industries, Mk 40 e-beam evaporator) techniques. The thickness of the buffer and catalyst layers is 10nm and 1nm respectively. CVD of CNT pillars is performed using a mixture of ethylene (Matheson, 99.95% purity) and hydrogen (Airgas, 99.999% purity) in a 1-inch tube furnace (Lindberg Blue M, Mini Mite). Details of the CVD condition are described elsewhere [21-23]. The height of CNT pillars used in this study is varied between 200 μm and 800 μm. The as-grown CNT pillars used in this study are in the shape of a hollow cylindrical pillar with outer and inner diameters of 50–150 μm and 25–120 μm respectively.

After fabrication, CNT pillars are exposed to oxygen plasma treatment using a remote RF oxygen plasma etcher (PVA Tepla, M4L) at a power setting of 50 W, an oxygen flow rate of 100–150 sccm, and a chamber pressure of 500 mTorr [22]. The as-grown CNT pillars, together

with their growth substrates, are placed at the center of the chamber to ensure the uniformity of plasma exposure during the oxidation process. The exposure time is varied between 1 and 20 minutes.

Changes in macroscopic morphology of CNT pillars are characterized using a field emission scanning electron microscope (Zeiss, 1550 VP). Scanning electron micrographs are taken at a sample tilt angle of 60° using an acceleration voltage of 5 kV. Local oxygen to carbon atomic ratio (O/C) is measured on specific CNT pillars by performing energy dispersive x-ray spectroscopy (EDS) (Oxford, X-Max Silicon Drift Detector) at an acceleration voltage of 5 kV. Changes in the microscopic structure of CNT pillars are characterized using a high performance transmission electron microscope (FEI, Tecnai F30UT). Transmission electron micrographs and selected area diffraction pattern (SADP) are collected with an acceleration voltage of 300 kV. For TEM and SADP, each sample is prepared by scraping off a small amount of CNT pillars from their growth substrates and dispersing the CNTs in ethanol (Sigma Aldrich, 200 proof) under sonication for 5 minutes. This dispersion is then poured on a holey carbon grid (Electron Microscopy Sciences, C-Flat) and dried in low vacuum at room temperature.

Surface chemistry characteristics of CNT pillars are assessed using x-ray photoelectron spectroscopy (XPS) (Surface Science, M-Probe XPS). A monochromatic 1486.6 eV Al Kα is used as the x-ray source and the detailed C1s spectra are collected at a binding energy of 281–297 eV and a spot size of 100 µm. Each sample is prepared from the dispersion of CNT pillars mentioned above, which is then poured uniformly on a clean silicon chip and dried in low vacuum at room temperature. Changes in relative surface concentration of various C bonds are quantified by performing deconvolution on the C1s spectra using Gaussian-Lorentzian peak fitting with Shirley baseline correction at the following binding energies: C-C sp2: 284.7 ± 0.1

eV (FWHM 0.9 eV), C-C sp3: 285.6 ± 0.1 eV (FWHM 1.3 eV), C-O: 286.6 ± 0.1 eV (FWHM 1.4 eV), C=O: 287.4 ± 0.2eV (FWHM 1.4 eV), O-C=O: 289 ± 0.4 eV (FWHM 1.7 eV), O-C(O)=O: 290.4 ± 0.4 eV (FWHM 1.7 eV), and π- π*: 292.1 ± 0.4 eV (FWHM 1.6 eV) [13, 17, 23].

Raman spectroscopy characterization is performed using a micro Raman spectrometer system (Renishaw, M1000) equipped with an argon ion laser at an excitation wavelength of 514.5 nm. Each sample is characterized as is without prior sample preparation. Raman spectra are collected using an optical magnification of 100X in a non-polarized mode at a Raman shift of 500–3500 cm^{-1}. Three CNT signature peaks are identified at ~1350cm^{-1} (D band), ~1585cm^{-1} (G band), and ~2695 cm^{-1} (G' band) [24, 25]. The quality of CNT pillars is quantified by the ratio between the integrated area under the D band and the G band (I_D/I_G).

3. Results

3.1. CNT Pillar Morphology

SEM images show that oxygen plasma treatment has the capability to modify the macroscopic morphology of hollow cylindrical CNT pillars across large samples (Figure 1a). Upon exposure to oxygen plasma treatment, a tapered geometry is effectively introduced to each CNT pillar. This taper geometry becomes more pronounced as the oxygen plasma exposure increases (Figure 1b). The base diameter of the pillar remains constant while the tip diameter progressively shrinks with increasing plasma exposure. The tapering effect is generally uniform over the height of the pillar, making the tip of the pillar as the location where the pillar diameter reaches a minimum value. However, at high plasma doses, the minimum diameter point in the pillar shifts from the tip to slightly below the tip, forming an observable neck just below the tip.

Similarly, the wall thickness of the pillars gradually decreases with increased oxygen plasma exposure. It follows, generally, that the point of minimum wall thickness in the pillar corresponds to the location of minimum diameter either at the tip of the pillar for low dosage treatments or at the neck of the pillar for high dosage treatments.

The morphological evolution of the CNT pillar as it undergoes increasing oxygen plasma exposure can be observed by correlating its minimum diameter and wall thickness to the oxygen adsorbates concentration of the pillar (Figure 2a). Oxygen adsorbates concentration, which indicates the total dose received by a CNT pillar over the cumulative oxygen plasma exposure, can be estimated by its oxygen to carbon ratio (O/C ratio) as measured through EDS. It has been widely known that plasma treatment is dependent on a number of physical parameters, including plasma flow rate and density, chamber pressure, power setting, and exposure time. In this study, O/C ratio is chosen as a single robust parameter to characterize the plasma treatment process, allowing the morphological evolution of the CNT pillar to be significantly simplified. To clearly show the evolution, the minimum diameter (d_m) and wall thickness (t) of each CNT pillar are normalized by its original outer diameter (d_0) and wall thickness (t_0) respectively (Figure 2b). Three distinct phases of macroscopic morphological change are identified for the oxygen plasma treatment of CNT pillars.

Phase I is observed at a very low oxygen plasma dose, with a measured O/C below 4%, where changes in CNT pillar morphology are minimal (Figure 2a). While a small change in t/t_0 is apparent, changes in d_m/d_0 are primarily negligible. This indicates that the wall thickness is more responsive, albeit slightly, to the effect of oxygen plasma treatment than the minimum diameter. The correlation between d_m/d_0 and t/t_0 shows that the diameter remains constant until the wall thickness reaches about 80% of its original value (Figure 2c). Phase II is observed at a moderate

dose of oxygen plasma, where changes in morphology become more apparent (Figure 2a). Both d_m/d_0 and t/t_0 decrease proportionally with the increase of O/C. The reduction rate of both d_m/d_0 and t/t_0 is considerably high such that their values drop to less than 10% as the O/C of the pillar increases to about 10%. Here, the diameter and thickness of the pillar contract at similar rates during plasma treatment (Figure 2c).

Phase III is observed at an even higher dose of oxygen plasma, with a measured O/C ratio above 10%, where changes to d_m/d_0 and t/t_0 are not as apparent as in Phase II (Figure 2a). Indeed, both d_m/d_0 and t/t_0 continue to decrease to nearly 0% as the O/C of the pillar increases to 35%. However, it has to be noted that other modes of morphology modification appear in this regime. As the base of the CNT pillar begins to collapse, formerly vertical CNTs now run horizontal across the substrate before coming together to support the pillar with a much reduced base diameter. Also in Phase III, formation of a neck is observable just below the tip of the CNT pillar. The neck of the pillar represents the boundary between the crust and vertically aligned CNTs. Just prior to the formation of the neck, at the end of Phase II, the tip loses its circular shape which indicates the highly pliable state of the pillar tip. It is observed that the crust layer reaches a minimum feature size while the rest of the pillar continues to contract below the crust (Figure 2d). As the diameter of the neck continues to shrink, the CNTs that support the tip begin to bend causing the tip of the pillar to expand outward creating a flower-like bloom. This flower-like bloom created at the tip remains constant in size throughout Phase III.

In comparing the transition points for d_m/d_0 and t/t_0, as approximated by a linear fit to the data, it is observed that for both the transition from Phase I to Phase II and the transition from Phase II to Phase III, the transition in wall thickness and minimum diameter occurs almost simultaneously. For the transition from Phase I to Phase II, the transition in t/t_0 and d_m/d_0 occurs

at an O/C of about 3.2% and 3.8% respectively. For the transition from Phase II and Phase III, the transition in t/t_0 and d_m/d_0 occurs at an O/C of about 9.6% and 10.2% respectively. This indicates that the decrease in t/t_0 is followed immediately by a decrease in d_m/d_0. A single linear fit can be used to approximate the change in d_m/d_0 with respect to the change in t/t_0 in both Phase II and Phase III. This demonstrates that despite significant changes in the macroscopic behavior of pillar contraction between Phase II and Phase III, the relative relation between minimum diameter and wall thickness remains the same throughout Phase II and III (Figure 2c).

The pillars are most responsive to the oxygen plasma treatment in the dosage range represented by Phase II. In Phase II, the tip diameter can be controllably reduced to about 93% of its original size without the complication of artifacts such as neck formation and base collapse as observed in Phase III. The progression in the profile of the pillars can be modeled as a hyperbolic cosine such that the nanotubes comprising the pillar are represented as a set of aligned, similar curves (Figure 3a). In this representation, the CNTs before the plasma treatment are modeled as perfectly vertical. The CNTs in the model are constrained as having a constant arc length and a fixed position on the substrate (Figure S1 in the Supplementary Material). Both of these constraints follow from experimental observations of the pillar during shape transformation. Due to the fixed position of the CNTs at the base, the effect of oxygen plasma treatment is more apparent near the tip, resulting in the overall concave appearance of the resulting CNT pillar (Figure S2 in the Supplementary Material).

In addition to predicting the profile of the pillar, the model allows for insight into the correlation between pillar height and tip diameter during the oxygen plasma treatment (Figure 3c). Here, the pillar height (h) and tip diameter (d_t) of each CNT pillar are normalized by its original dimensions (h_0 and d_0 respectively) before treatment (Figure 3d). The end of Phase II

itself is depicted in the final pillar profile with d_t/d_0 of 10%. It is found that the overall change in h/h_0 during the oxygen plasma treatment depends greatly on h_0. In the span of the plasma treatment, d_t/d_0 decreases by more than 93%. However, for pillars of with h_0 of 200 µm and 400 µm, the decrease in h/h_0 is limited to about 11% and 3% respectively (Figure 3b). This demonstrates that d_t/d_0 decreases at a much faster rate than h/h_0 (Figure 3c).

3.2. CNT Structure

Changes in morphology of CNT pillars due to oxygen plasma treatment can be related to structural changes of CNTs at a smaller length scale. High magnification SEM images show that a low oxygen plasma dose does not have a significant effect on the CNT inter-tube spacing and packing density (Figure 4a). Indeed, the vertical alignment and inter-tube spacing of the as-grown CNT pillars are similar to the pillars at the transition point between Phase I and Phase II. However, in Phase II, the CNT inter-tube spacing decreases with increased oxygen plasma exposure, suggesting the presence of a CNT densification process. In this phase, the CNTs are packed in a much smaller space such that their entanglement and curliness start to disappear. A further increase in oxygen plasma exposure results in an additional reduction of inter-tube spacing. Thus, in Phase III, each individual CNT is in such close contact with its neighboring CNTs that the empty space between each CNT can no longer be observed by SEM.

Furthermore, high magnification TEM images indicate that the graphitic structure of each CNT undergoes a significant transformation during the oxygen plasma treatment (Figure 4b). The originally thin, amorphous structure that encapsulates the highly graphitic structure of the as-grown CNT becomes thicker as the oxygen plasma dose increases. Indeed, at the transition point from Phase I to Phase II, the thickness of this amorphous structure is about the same as that

of the CNT side wall. Note that the original graphitic structure of the CNT is still largely intact at the beginning of Phase II. However, a further increase in the plasma exposure results in the disappearance of such amorphous coating. In Phase II, the formation of holes on the CNT side wall that are several layers deep becomes more apparent and the graphitic structure of the CNT is no longer intact. At an even higher exposure, significant deformation to the graphitic structure of the CNT becomes more pronounced. Indeed, in Phase III, the remaining structure of the CNT becomes amorphous and the well-organized graphitic stacking of the CNT wall completely disappears.

The above mentioned structural transformation is further confirmed by changes in the SADP relative intensity of CNTs during the oxygen plasma treatment (Figure 4c). The observed concentric circular SADP of as-grown CNTs originates from the multiple orientations of the CNT walls. The first feature (A) and the third feature (C) at a spacing of 2.9 nm^{-1} and 5.9 nm^{-1}, respectively, indicate the <0002> and <0004> orientations, which are associated with the graphitic stacking of the CNT wall [26]. The second feature (B) and the fourth feature (D) at spacing of 4.9 nm^{-1} and 8.4 nm^{-1}, respectively, indicate the $<10\bar{3}0>$ and $<11\bar{2}0>$ orientations, which are associated with the hexagonal lattice of the C-C sp2 hybridized carbon structure. The SADP of CNTs at the beginning of Phase II is similar to that of CNTs in Phase I but with more dispersed features. This confirms the TEM observation that a low dose of oxygen plasma exposure results in an encapsulation of CNTs by thick amorphous coatings without severely damaging their graphitic structures [27]. The SADP of CNT pillars in Phase II and III indicate a complete disappearance of feature C, while feature B can still be observed. Moreover, feature A is now similar to the pattern of amorphous structure and is no longer distinguishable. This

confirms the TEM observation that a high dose of oxygen plasma results in the disappearance of well-organized graphitic stacking of the CNT wall.

The increase in defect density induced by oxygen plasma treatment is further verified by the increase in I_D/I_G obtained from Raman spectroscopy (Figure 4d). As expected, the I_D/I_G of CNT pillars increases with the increase of oxygen plasma exposure. The I_D/I_G increases from about 1 for the as-grown CNT pillars to about 1.3 for the CNT pillars at the beginning of Phase II. In Phase II, the I_D/I_G increases even further, up to a maximum of 1.5. Such a high I_D/I_G value indicates that CNTs in Phase II are highly defective due to the formation of holes on the CNT side wall. Interestingly, further exposure to the oxygen plasma treatment results in a decrease of I_D/I_G, where the I_D/I_G of CNT pillars in Phase III is found to be about 1.3. However, such decrease in I_D/I_G is accompanied by the appearance of a shoulder D' peak (~1620cm^{-1}), a blue shift in both D and G bands, and the complete disappearance of G' band. These changes can all be attributed to a significant increase in disorder-induced strain and scattering of the CNT π-bond network [28-30]. These changes also imply that the remaining graphitic structures are heavily doped with oxygen adsorbates [16, 20, 31, 32].

XPS analysis is performed to further elucidate the evolution of structural transformation of CNT pillars as they are being exposed to an increasing dose of oxygen plasma (Figure 5a). As expected, the C1s spectra of as-grown CNT pillars exhibit an extremely strong C-C sp2 peak and a considerably weak C-C sp3 peak. In addition, C-O, C=O, O-C=O, O-C(O)-O, and π- π* shakeup peaks are almost nonexistent. In Phase I, the intensity of oxygenated groups and C-C sp3 peaks increases slowly with the increase of oxygen plasma exposure. However, they are consistently observed to be considerably weaker than the C-C sp2 peak. The C1s spectra in Phase 1 are still strongly influenced by the C-C sp2 peak. Beyond this threshold, the intensity of

oxygenated groups and C-C sp3 peaks start to increase rapidly with the increase of oxygen plasma exposure. Note that the intensity of the C-O and O-C=O peaks increases at a considerably faster pace than that of the C=O and O-C(O)-O peaks, and that the intensity of the C-C sp3 peak increases at an even faster rate (Figure 5b). At the beginning of Phase II, the intensity of C-C sp3 peak is already about the same as that of C-C sp2 peak.

A more dramatic transformation can be observed during Phase II, where the C1s spectra are no longer dominated by the C-C sp2 peak (Figure 5a). Notice that the C1s spectra are now dominated by the C-O peak. In fact, the intensity of C-O peak may reach up to three times higher than that of the C-C sp2 peak. Thus, the peak position of C1s spectra is now shifted to a binding energy of 286.6 eV. The C-C sp2 peak starts to disappear at a higher dose of oxygen plasma treatment. At the end of Phase II, the intensity of the C-C sp2 peak has become extremely weak, followed by the rapid emergence of the C=O, O-C=O, and O-C(O)-O peaks (Figure 5b). Here, the peak position of the C1s spectra is shifted to an even higher binding energy of 288.6 eV. Further increase in oxygen plasma exposure results in the disappearance of the C-O bond, while the intensity of the C=O, O-C=O, and O-C(O)-O peaks continues to increase. In Phase III, the intensity of the C-C sp2 peak is negligible, suggesting that the remaining C-C bonds are in the form of sp3 hybridization.

4. Discussion

As described earlier, CNT pillars undergo three distinct phases of structural and morphological evolution as they are subjected to an increasing dose of oxygen plasma (Figure 6). The first phase (Phase I) occurs at a very low dose of oxygen plasma, and is indicated by the absence of changes in the large-scale morphology of CNT pillars. Here, the morphology of the

CNT pillars remains similar to that of the as-grown CNT pillars. The second phase (Phase II) occurs at a moderate oxygen plasma dosage, and is indicated by a major transformation in the macroscopic morphology of the CNT pillars. Such a major transformation can be easily observed from the rapid decrease in wall thickness and diameter of the CNT pillar with increasing oxygen plasma exposure. The final phase (Phase III) occurs at a high dose of plasma treatment, and is indicated by macroscopic morphological changes including collapse of the base of the pillar and formation of a neck below the tip of the CNT pillar.

In Phase I, the effect of oxygen plasma treatment on CNT pillars is limited primarily to functionalization of the CNTs. In this phase, oxygen radicals are adsorbed by CNTs mainly in the form of hydroxyl, epoxide, and carbonyl groups (Figure 5b). It has been known that these groups are readily formed in stable configurations on the outer surface and defect sites of graphitic structures during oxygen plasma treatment [13, 17, 33]. Generally, hydroxyl groups are formed on the CNT walls by a reaction between physisorbed water molecules and oxygen radicals produced by the plasma treatment. On sites that are free from physisorbed water, oxygen radicals are commonly adsorbed as epoxide groups due to their lowest energy configuration. Because epoxide groups have a tendency to create pair structures, some of these groups subsequently form neighboring carbonyl groups. Unlike the formation of hydroxyl and carboxyl groups that are relatively superficial, the formation of carbonyl groups gives rise to structural defects and holes. Although the formation of these groups induces a transformation in carbon hybridization from sp2 to sp3, their relative concentration is rather low such that the graphitic structure of the CNT appears to be reasonably intact.

In addition to surface functionalization, surface encapsulation by amorphous structures also occurs in this phase (Figure 4b). Such amorphous structures are most likely formed by

redeposition of some organic compounds during oxygen plasma treatment [27]. It has been known that a small amount of carbon can be easily etched from highly defective graphitic structures and inherently existing amorphous carbon by both physical bombardment of the plasma and chemical reaction with highly reactive oxygen radicals, even at a relatively low dosage of oxygen plasma treatment [20, 30, 34]. Note that the as-grown CNT pillars are not entirely free from structural defects and amorphous carbon coating (Figure 4b and Figure 4d). Further interactions with the complex plasma environment allow the etched carbon to be redeposited as amorphous organic compounds onto the CNT walls, either physically or chemically [15]. While the deconstruction of defective CNTs is not obvious, the redeposition of amorphous carbon during oxygen plasma treatment is conspicuous.

Despite the structural changes induced by functionalization and surface encapsulation processes, all macroscopic features of the CNT pillar, including diameter and wall thickness, remain unchanged in Phase I (Figure 2a). This implies that CNT densification does not occur in this phase, as observed from the unaltered CNT inter-tube spacing (Figure 4a). Although amorphous carbon and oxygen adsorbates increase the CNT surface energy, they are present in a low concentration that is inadequate to influence the interaction between neighboring CNTs in the pillar. The absence of changes in the macroscopic morphology also suggests that in this phase the etching process is essentially limited to the highly defective graphitic structures and inherently existing amorphous carbon.

In Phase II, changes in the CNT graphitic structure become more pronounced with increasing oxygen plasma exposure. The concentration of oxygen adsorbates is found to be increasing rapidly as the CNT pillars undergo a prolonged oxygen plasma treatment. In fact, even at the beginning of Phase II, CNT pillars are already functionalized by a high concentration of oxygen

adsorbates. In Phase II, oxygen is adsorbed in the form of not only hydroxyl, epoxide, and carbonyl groups, but also carboxyl and carbonate groups (Figure 5b). These later groups are typically formed by a rapid reaction between carbonyl groups and oxygen or hydroxyl radicals [13]. Since these groups are most likely formed at the edges of defect sites, their presence indicates the occurrence of a substantial etching process.

Note that the surface encapsulation processes by amorphous carbon cease to occur in Phase II. In fact, the thickness of the amorphous coating decreases rapidly with increasing dosage of oxygen plasma treatment. Since amorphous carbon more readily reacts with oxygen radicals than graphitic structures [20, 27], etching of the CNT is started by the removal of the amorphous coating. Once the amorphous coating has been largely removed, the CNT graphitic structure becomes susceptible to further functionalization and etching (Figure 4b). As a result, the remaining CNTs undergo a major transformation in terms of carbon hybridization, from sp2 dominated structure to sp3 dominated structure (Figure 5a). This transformation induces additional strain to the CNT structure due to the difference in C-C bond length from trigonal planar sp2 carbon hybridization to tetragonal sp3 carbon hybridization, and further intensify the degree of disorder in the CNT π-bond network (Figure 4d) [33, 35].

A further increase in the concentration of oxygenated groups also leads to an increase in the magnitude of the CNT surface charge and energy, which ultimately increases the attraction between individual CNTs in the pillar. As a result, the densification process starts to occur, which is indicated by the decrease in the CNT inter-tube spacing (Figure 4a). The densification process has also been regarded as an effective means to further decrease the CNT surface energy [15, 18]. This densification process in turn triggers the macroscopic shape change as observed in the cylindrical CNT pillar by a reduction in the pillar thickness quickly followed by reduction in

tip diameter. Because the availability of oxygen radicals at the tip of the CNT pillar is generally higher than on the side of the pillar, the rate of functionalization and etching at the tip is relatively higher than that at the side wall of the CNT [15, 36]. Thus, the densification process at the tip of the CNT pillar occurs at a higher rate than at the side of the pillar, resulting in the formation of a tapered geometry on the cylindrical CNT pillar. A combination of CNT etching and densification processes are regarded as the underlying mechanism of change in macroscopic CNT pillar morphology that occurs in Phase II.

In Phase III, the prolonged exposure to oxygen plasma results in excessive etching of the CNT walls, which gives rise to the formation of large holes that are several layers deep. Some of the CNTs are even found with walls that are almost completely etched or have become amorphous (Figure 4b). The CNT densification process continues during this phase resulting in an even higher CNT packing density. Here, each remaining CNT is in close contact with its neighbors and the empty space between these remaining CNTs can hardly be observed (Figure 4a). The effect of such extensive etching and densification processes on the large scale morphology of CNT pillars can be observed from the further decrease in diameter and wall thickness, as well as the collapse of the base. In addition, neck formation near the pillar tip becomes more apparent in Phase III. This necking effect is mainly caused by the presence of a crust region, several microns thick, at the tip of the pillar. In the crust region, the alignment of the CNTs breaks down creating a dense layer of highly entangled CNTs, which is often accompanied by a thick layer of amorphous carbon as well as residual metal catalyst and oxides buffer depending on the quality of the CNT growth. Thus, the crust region is generally more resistant to the effect of oxygen plasma treatment than the rest of the CNT pillar. The formation

of a neck near the tip of the CNT pillar ultimately results in a morphological transformation similar to a blooming flower (Figure 2d).

The geometric model introduced in this study can be used as a guide to predict the evolution of the CNT pillar profile during shape transformation in Phase II. The good agreement between the model and experimental observation proves that the CNT pillar profile can indeed be represented as a smooth curve derived from a hyperbolic cosine function (Figure 3a). As depicted in the model, the profile of the pillar is initially linear and then becomes more concave as the oxygen plasma treatment progresses through Phase II. In Phase III, the model no longer captures the profile of the pillar as the profile can no longer be represented as a single global curve. Features such as necking at the tip and the collapse of the base create local deviations in the shape of the pillar. Comparing the predicted curve to the actual profile of a pillar at the verge of neck formation, the model captures the overall profile of the pillar with the exception of the top 20% of the pillar due to the formation of the neck, which abruptly changes the curvature of the pillar near the tip. It is also predicted by the model that oxygen plasma treatment slightly reduces the height of the cylindrical CNT pillar simultaneously with rapid reduction in tip diameter. This suggests that a highly tapered CNT pillar can be fabricated without sacrificing its initial height. While the change in height of the CNT pillar during oxygen plasma treatment can be neglected for taller pillars, change in height for shorter CNT pillars can be significant (Figure 3c). The model ultimately demonstrates the ability to accurately tailor the morphology of a treated pillar based on the pillar's initial morphology and its total oxygen plasma dosage. Thus, oxygen plasma treatment represents a significant step towards creating scalable, fully three-dimensional CNT structures.

As described herein, oxygen plasma treatment represents a powerful means to engineer the morphology of CNT pillars into complex geometries. Traditional bottom-up fabrication methods, including catalyst patterning and chemical vapor deposition, restrict the pillar geometry to a constant cross-section. This restriction ultimately limits the widespread adaptation of CNT pillars for numerous applications. As described here, oxygen plasma treatment can be utilized as a simple and scalable method for overcoming this obstacle by enabling three-dimensional modification to the geometry of CNT pillars without inducing excessive damage to the CNT graphitic structure. Oxygen plasma treatment can be easily utilized to introduce a tapered geometry to the cylindrical CNT pillar by reducing the tip diameter by up to 93%. Since most changes in large scale morphology of CNT pillars take place in Phase II, it represents the ideal treatment conditions without the complication of non-uniform artifacts such as excessive neck formation and base collapse as observed in Phase III (Figure 6). In fact, for most practical applications, it may be beneficial to stop the oxygen plasma treatment before reaching Phase III. While Phase III offers even more unique shape transformations, such as a blossoming-type transformation of the CNT pillar tip, it also results in the excessive etching and amorphization of the CNT graphitic structures. Therefore, Phase III of the oxygen plasma treatment may not be suitable for applications that rely on the inherent properties of CNTs.

5. Conclusion

The findings presented herein demonstrate the potential of oxygen plasma treatment as a post-growth fabrication technique to engineer the macroscopic morphology of vertically-aligned CNT structures. In particular, oxygen plasma treatment has the capability to introduce a tapered geometry to hollow cylindrical CNT pillars by controllably reducing the tip diameter by up to 93%. Changes in morphology of a CNT pillar during the oxygen plasma treatment can be

approximated by a geometric model based on a hyperbolic cosine function. As predicted by the model, the profile of the CNT pillar is initially linear and then becomes more concave as the oxygen plasma treatment progresses. All macroscopic features of the CNT pillar, including diameter, wall thickness, and height, are found to be proportionally decreasing with increasing oxygen plasma dosage.

Changes in macroscopic morphology of CNT pillars can be related to structural changes on the length scale of individual CNTs. These changes can be qualitatively categorized into three distinct phases representing increasing dosages of oxygen plasma treatment. At a low dose of plasma treatment (Phase I), the effect of the treatment on CNT pillars is limited primarily to functionalization of the CNTs. As observed experimentally, macroscopic changes in morphology are the result of a combination of CNT etching and densification processes and occur primarily at a moderate dosage of oxygen plasma (Phase II). A high dose of plasma treatment (Phase III) results in the excessive etching and amorphization of the CNT graphitic structures. Therefore, moderate doses of oxygen plasma treatment, as represented by Phase II, represent the ideal conditions to introduce controllable changes in the macroscopic morphology of CNT pillars without the complication of non-uniform artifacts such as neck formation and base collapse that are observed at larger doses of plasma treatment.

Acknowledgement

This work was supported by ZCube s.r.l. The authors acknowledge the support and infrastructure provided by the Charyk Laboratory for Bio-Inspired Design, the Kavli Nanoscience Institute, the Molecular Materials Research Center of the Beckman Institute, and the Geology and Planetary

Sciences Analytical Facility of the California Institute of Technology. The authors also acknowledge Prof. George Rossman for providing an access to the Raman spectrometer.

Reference

[1] De Volder MF, Tawfick SH, Baughman RH, Hart AJ. Carbon nanotubes: present and future commercial applications. Science. 2013;339(6119):535-9.

[2] Saleem AM, Berg J, Desmaris V, Kabir M. Nanoimprint lithography using vertically aligned carbon nanostructures as stamps. Nanotechnology. 2009;20(37):375302.

[3] Lyon BJ, Aria AI, Gharib M. Feasibility Study of Carbon Nanotube Microneedles for Rapid Transdermal Drug Delivery. MRS Online Proceedings Library. 2013;1569.

[4] Lyon BJ, Aria AI, Gharib M. Fabrication of carbon nanotube—polyimide composite hollow microneedles for transdermal drug delivery. Biomedical Microdevices. 2014:1-8.

[5] Jung YC, Bhushan B. Mechanically Durable Carbon Nanotube−Composite Hierarchical Structures with Superhydrophobicity, Self-Cleaning, and Low-Drag. ACS Nano. 2009;3(12):4155-63.

[6] Zhu L, Xiu Y, Xu J, Tamirisa PA, Hess DW, Wong C-P. Superhydrophobicity on Two-Tier Rough Surfaces Fabricated by Controlled Growth of Aligned Carbon Nanotube Arrays Coated with Fluorocarbon. Langmuir. 2005;21:11208-12.

[7] Wang T, Jeppson K, Ye L, Liu J. Carbon-Nanotube Through-Silicon Via Interconnects for Three-Dimensional Integration. Small. 2011;7(16):2313-7.

[8] Nicolo' C, Sugiura M, Yusaku K, Yunlong L, Kai A, Olivier R, et al. Measuring the electrical resistivity and contact resistance of vertical carbon nanotube bundles for application as interconnects. Nanotechnology. 2011;22(8):085302.

[9] Yan X, Tay B-K, Miele P. Field emission from ordered carbon nanotube-ZnO heterojunction arrays. Carbon. 2008;46(5):753-8.

[10] Lee DH, Lee JA, Lee WJ, Kim SO. Flexible Field Emission of Nitrogen-Doped Carbon Nanotubes/Reduced Graphene Hybrid Films. Small. 2011;7(1):95-100.

[11] Wang W, Ruiz I, Ahmed K, Bay HH, George AS, Wang J, et al. Silicon Decorated Cone Shaped Carbon Nanotube Clusters for Lithium Ion Battery Anodes. Small. 2014:n/a-n/a.

[12] Kang C, Baskaran R, Hwang J, Ku B-C, Choi W. Large scale patternable 3-dimensional carbon nanotube–graphene structure for flexible Li-ion battery. Carbon. 2014;68(0):493-500.

[13] Aria AI, Gani AW, Gharib M. Effect of dry oxidation on the energy gap and chemical composition of CVD graphene on nickel. Appl Surf Sci. 2014;293(0):1-11.

[14] Tomlin NA, Curtin AE, White M, Lehman JH. Decrease in reflectance of vertically-aligned carbon nanotubes after oxygen plasma treatment. Carbon. 2014;74(0):329-32.

[15] Hou Z, Cai B, Liu H, Xu D. Ar, O2, CHF3, and SF6 plasma treatments of screen-printed carbon nanotube films for electrode applications. Carbon. 2008;46(3):405-13.

[16] Chen C, Liang B, Ogino A, Wang X, Nagatsu M. Oxygen Functionalization of Multiwall Carbon Nanotubes by Microwave-Excited Surface-Wave Plasma Treatment. J Phys Chem C. 2009;113(18):7659-65.

[17] Naseh MV, Khodadadi AA, Mortazavi Y, Pourfayaz F, Alizadeh O, Maghrebi M. Fast and clean functionalization of carbon nanotubes by dielectric barrier discharge plasma in air compared to acid treatment. Carbon. 2010;48(5):1369-79.

[18] Zhao B, Zhang L, Wang X, Yang J. Surface functionalization of vertically-aligned carbon nanotube forests by radio-frequency Ar/O2 plasma. Carbon. 2012;50(8):2710-6.

[19] Kalbacova M, Broz A, Kromka A, Babchenko O, Kalbac M. Controlled oxygen plasma treatment of single-walled carbon nanotube films improves osteoblastic cells attachment and enhances their proliferation. Carbon. 2011;49(9):2926-34.

[20] Liu Y, Liu L, Liu P, Sheng L, Fan S. Plasma etching carbon nanotube arrays and the field emission properties. Diamond Relat Mater. 2004;13(9):1609-13.

[21] Aria AI, Gharib M. Reversible Tuning of the Wettability of Carbon Nanotube Arrays: The Effect of Ultraviolet/Ozone and Vacuum Pyrolysis Treatments. Langmuir. 2011;27(14):9005-11.

[22] Aria AI, Gharib M. Dry Oxidation and Vacuum Annealing Treatments for Tuning the Wetting Properties of Carbon Nanotube Arrays. J Vis Exp. 2013:e50378.

[23] Aria AI, Gharib M. Physicochemical Characteristics and Droplet Impact Dynamics of Superhydrophobic Carbon Nanotube Arrays. Langmuir. 2014;30(23):6780-90.

[24] Dresselhaus MS, Jorio A, Hofmann M, Dresselhaus G, Saito R. Perspectives on Carbon Nanotubes and Graphene Raman Spectroscopy. Nano Lett. 2010;10(3):751-8.

[25] Dresselhaus MS, Jorio A, Saito R. Characterizing Graphene, Graphite, and Carbon Nanotubes by Raman Spectroscopy. Annu Rev Condens Matter Phys. 2010;1(1):89-108.

[26] Mattson EC, Pu H, Cui S, Schofield MA, Rhim S, Lu G, et al. Evidence of Nanocrystalline Semiconducting Graphene Monoxide during Thermal Reduction of Graphene Oxide in Vacuum. ACS Nano. 2011;5(12):9710-7.

[27] Xu T, Yang J, Liu J, Fu Q. Surface modification of multi-walled carbon nanotubes by O2 plasma. Appl Surf Sci. 2007;253(22):8945-51.

[28] Mehdi E, Wen-Wen W, Mohammad K, Yoshio S. Mechanically reliable thermoelectric (TE) nanocomposites by dispersing and embedding. Science and Technology of Advanced Materials. 2014;15(1):014201.

[29] Nourbakhsh A, Cantoro M, Vosch T, Pourtois G, Clemente F, Veen MH, et al. Bandgap opening in oxygen plasma-treated graphene Nanotechnology. 2010;21(43):435203-11.

[30] Yu K, Zhu Z, Zhang Y, Li Q, Wang W, Luo L, et al. Change of surface morphology and field emission property of carbon nanotube films treated using a hydrogen plasma. Appl Surf Sci. 2004;225(1–4):380-8.

[31] Kim DC, Jeon DY, Chung HJ, Woo Y, Shin JK, Seo S. The structural and electrical evolution of graphene by oxygen plasma-induced disorder; 2009.

[32] Chen C, Ogino A, Wang X, Nagatsu M. Plasma treatment of multiwall carbon nanotubes for dispersion improvement in water. Appl Phys Lett. 2010;96(13):131504-1131504-3.

[33] Suggs K, Person V, Wang X-Q. Band engineering of oxygen doped single-walled carbon nanotubes. Nanoscale. 2011;3(6):2465-8.

[34] Kim DC, Jeon DY, Chung HJ, Woo Y, Shin JK, Seo S. The structural and electrical evolution of graphene by oxygen plasma-induced disorder. Nanotechnology. 2009;20(37):375703.

[35] Muniz AR, Maroudas D. Hydrogenation effects on the structure and morphology of graphene and single-walled carbon nanotubes. J Appl Phys. 2010;108(11):113532.

[36] Huang S, Dai L. Plasma Etching for Purification and Controlled Opening of Aligned Carbon Nanotubes. The Journal of Physical Chemistry B. 2002;106(14):3543-5.

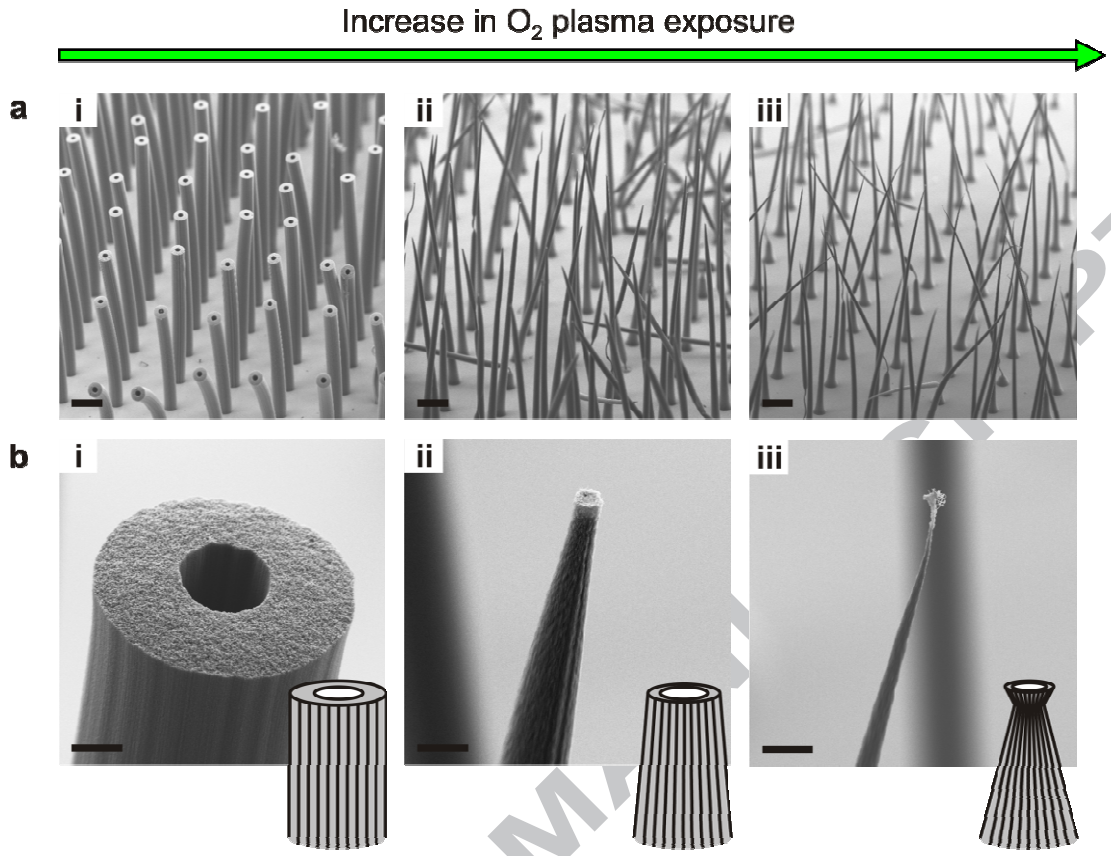

Figure 1. Low magnification (a) and high magnification (b) SEM images of CNT pillars with increasing oxygen plasma exposure. Changes in morphology can be observed as the as-grown CNT pillars (i) are treated with oxygen plasma with moderate exposure (ii) and heavy exposure (iii). Scale bars in (a) and (b) represent 100µm and 10µm respectively.

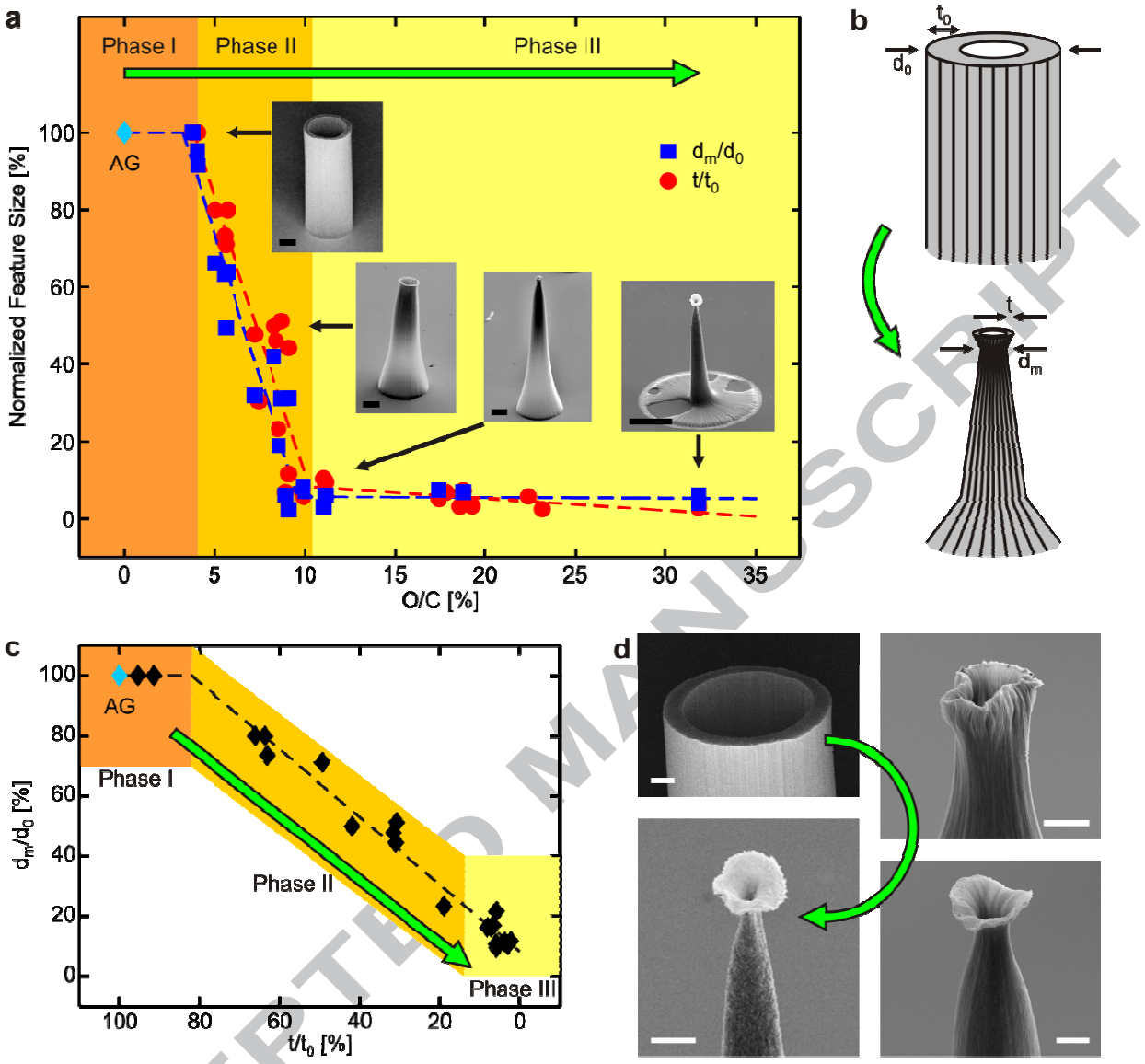

Figure 2. (a) Plot of normalized minimum diameter (d_m/d_0) and normalized thickness (t/t_0) versus O/C ratio of the CNT pillars as defined in the schematic (b). (c) Correlation between d_m/d_0 and t/t_0 with increasing oxygen plasma exposure. Three distinct behaviors (Phase I, Phase II, and Phase III) can be observed from (a) and (c). (d) The necking effect observed mainly in Phase II and III. Scale bars in (a) and (d) represent 50μm and 10μm respectively. AG denotes the as-grown CNT pillars.

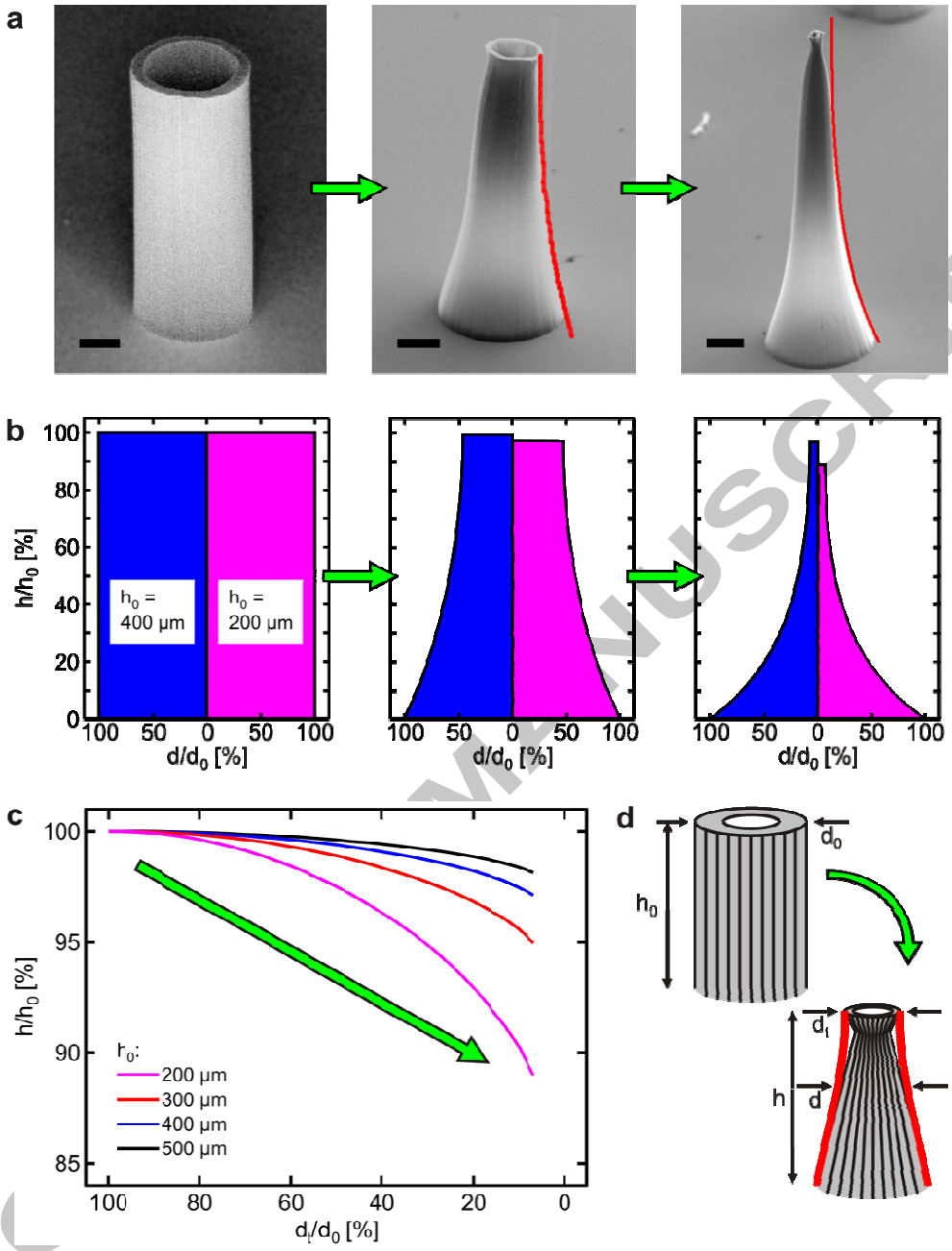

Figure 3. (a) Profile evolution of CNT pillars in Phase II and model prediction of the profile (represented by red lines). (b) The evolution of the model predicted profile of CNT pillars with initial height of 400µm and 200µm. (c) Plot of normalized pillar height (h/h_0) versus normalized tip diameter (d_t/d_0) with increasing oxygen plasma exposure as defined in the schematic (d). Scale bars in (a) represent 50µm.

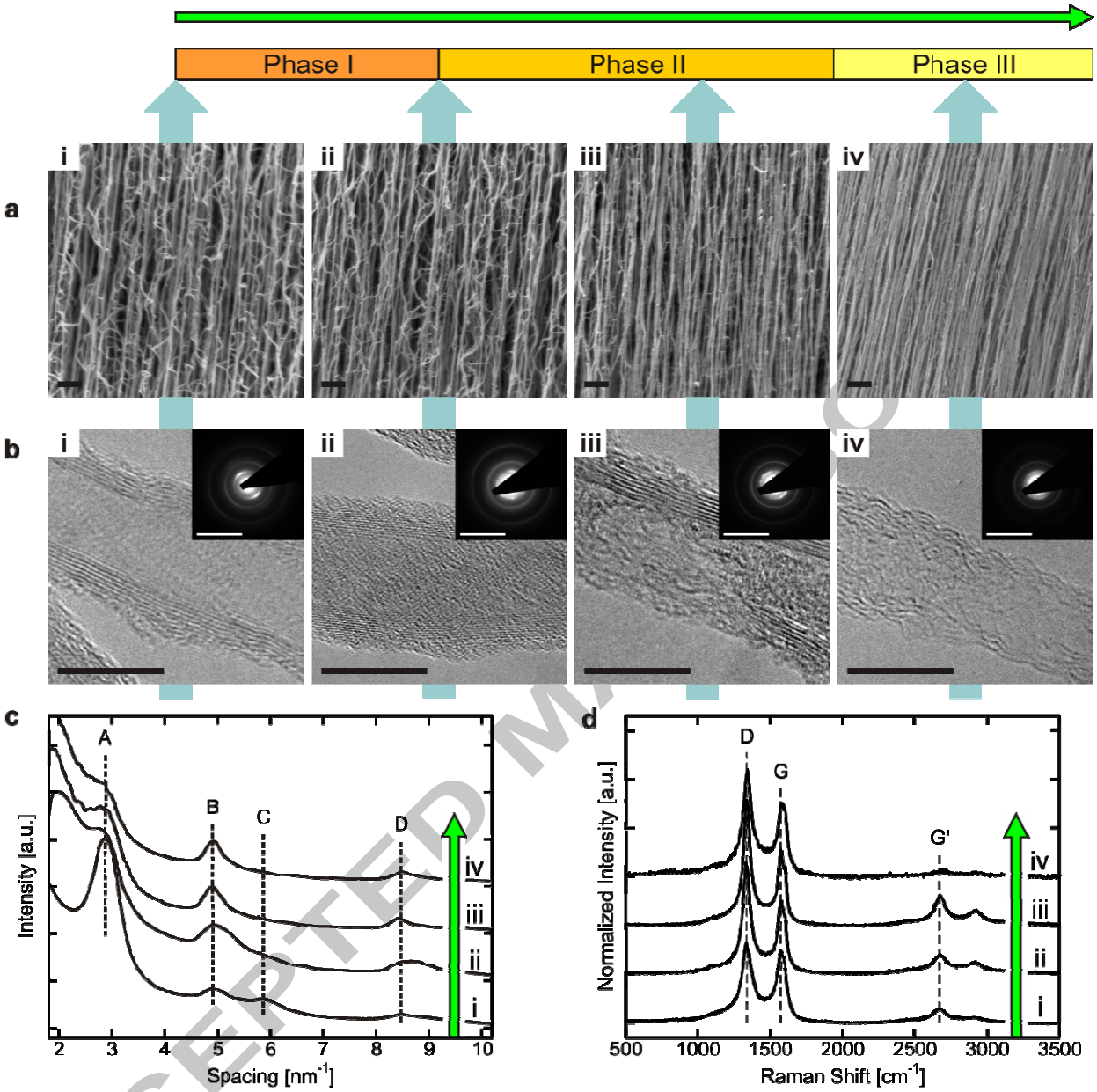

Figure 4. High magnification SEM images (a) and TEM images (b) of CNT pillars with increasing oxygen plasma exposure. Insets in (b) are selected area diffraction patterns of CNT pillars. (c) Diffraction pattern spacing obtained from (b) shows four distinct lines representing the <0002> (A), <1010> (B), <0004> (C), and <1120> (D) orientations. (d) Raman spectra of CNT pillars with increasing oxygen plasma exposure. (i) represents the as-grown CNT pillar, (ii) represents CNT pillar at the transition point between Phase I and Phase II, (iii) represents CNT

pillar in Phase II, and (iv) represents CNT pillar in Phase III. Scale bars in (a) and (b) represent 300 nm and 10nm respectively, and scale bars in insets of (b) represent $10nm^{-1}$.

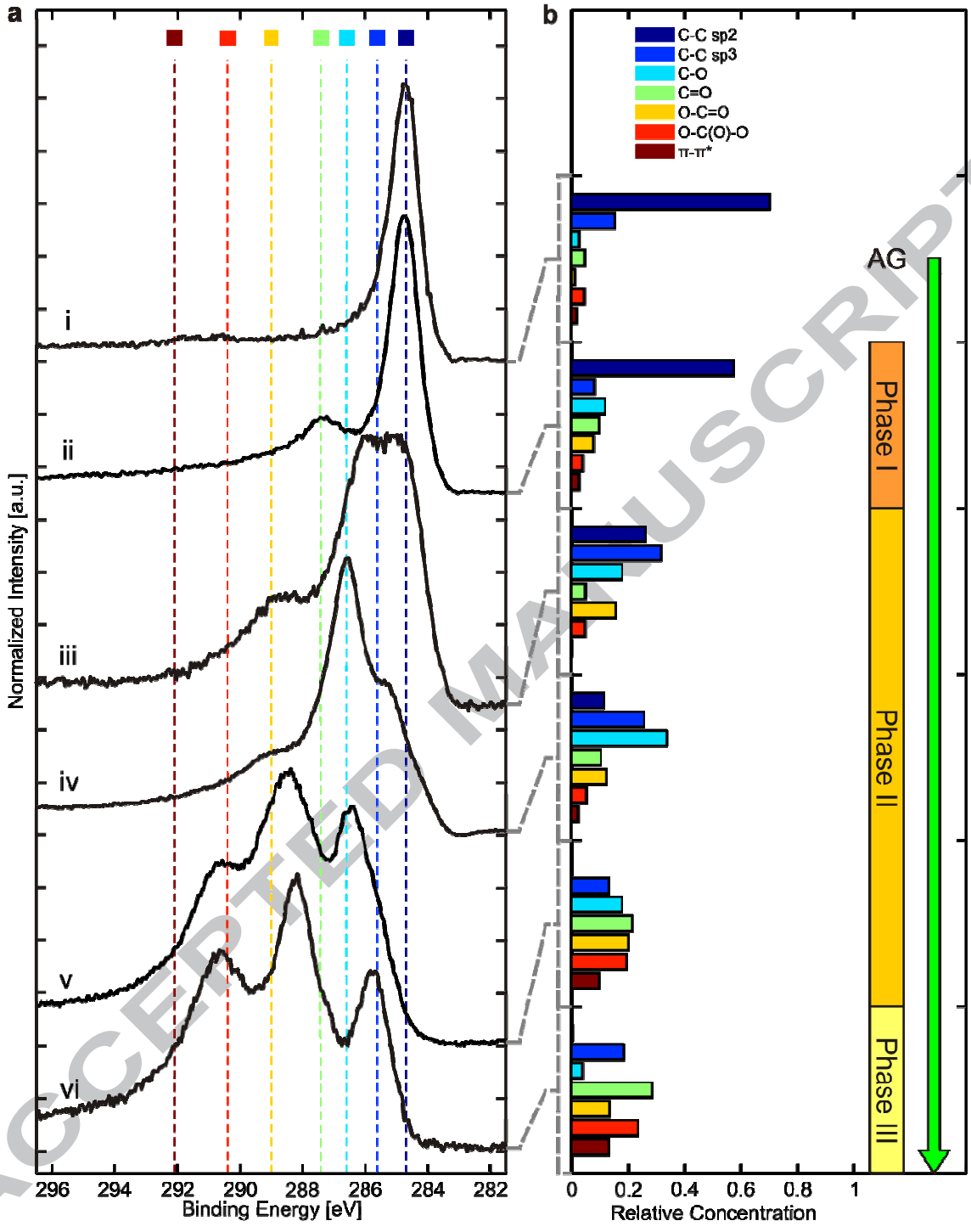

Figure 5. (a) XPS spectra of CNT pillars with different exposures to oxygen plasma treatment. A shift in C1s peak position to a higher binding energy is observable with increasing oxygen plasma exposure. (b) Relative concentration of C-C sp2, C-C sp3, C-O, C=O, O-C=O, O-C(O)-

O, and π- π^* shakeup obtained from (a). (i) represents the as-grown CNT pillar, (ii) represents CNT pillar in Phase I, (iii) represents CNT pillar at the beginning of Phase II, (iv) represents CNT pillar in Phase II, (v) represents CNT pillar at the end of in Phase II, and (vi) represents CNT pillar in Phase III. AG denotes the as-grown CNT pillars.

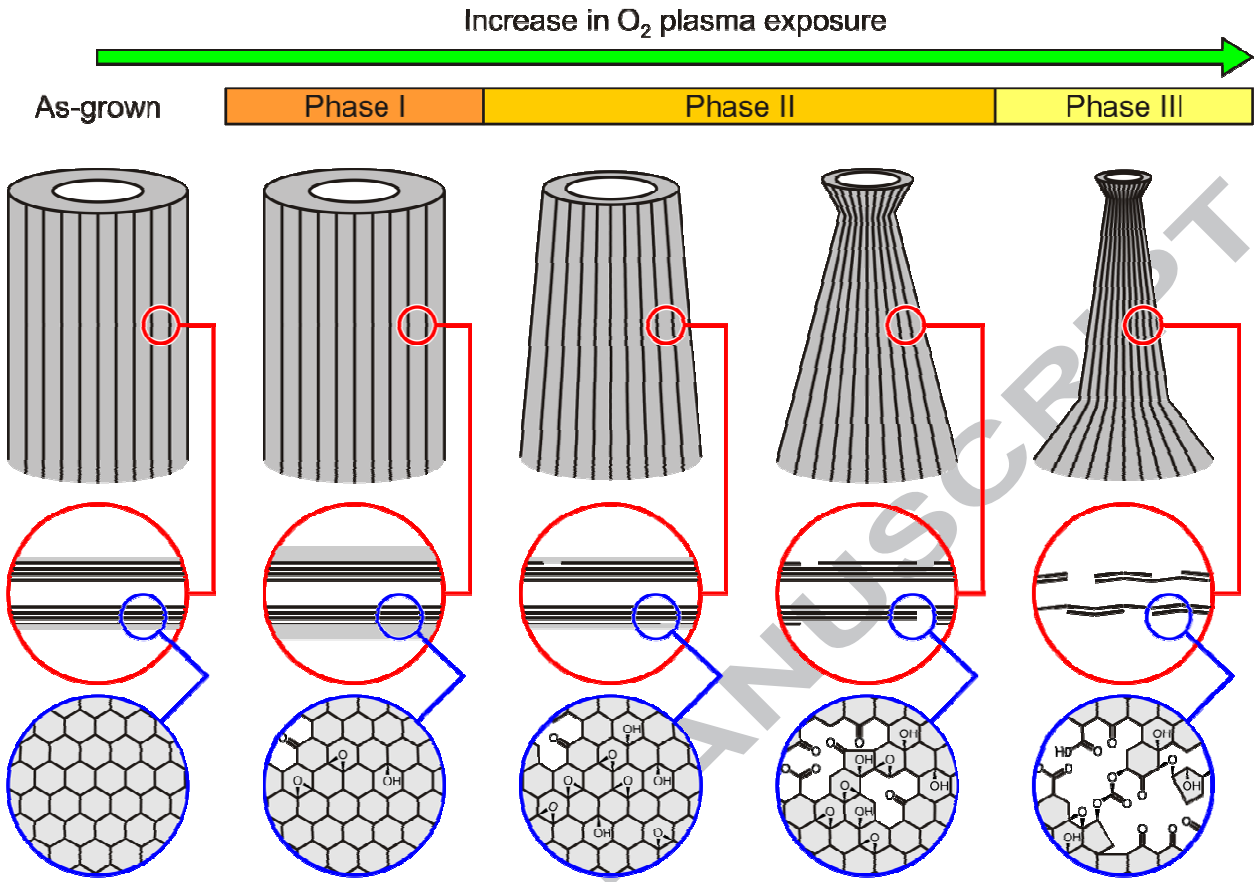

Figure 6. Schematic of the effect of oxygen plasma treatment to the macroscopic morphology and microscopic structure of CNT pillars. Phase I is limited primarily to functionalization of the CNTs. Phase II represents the ideal range to introduce modification to the macroscopic morphology of CNT pillars. Excessive CNT etching occurred in Phase III results in an extreme necking effect at the tip and collapse of the base.